Tuning the Dirac Point Position in $Bi_2Se_3(0001)$ via Surface Carbon Doping

Sumalay Roy,[1] H. L. Meyerheim,[1,*] A. Ernst,[1,2] K. Mohseni,[1] C. Tusche,[1] M. G. Vergniory,[1,3] T. V. Menshchikova,[1,4] M. M. Otrokov,[3,1,4] A. G. Ryabishchenkova,[4] Z. S. Aliev,[5] M. B. Babanly,[5] K. A. Kokh,[6] O. E. Tereshchenko,[7] E. V. Chulkov,[3,8] J. Schneider,[9] and J. Kirschner[1,10]

[1]*Max-Planck-Institut für Mikrostrukturphysik, Weinberg 2, D-06120 Halle, Germany*
[2]*Wilhelm-Ostwald-Institut für Physikalische und Theoretische Chemie, Universität Leipzig, Linnéstraße 2, 04103 Leipzig, Germany*
[3]*Donostia International Physics Center (DIPC), 20018 San Sebastián/Donostia, Spain*
[4]*Tomsk State University, 634050 Tomsk, Russia*
[5]*Baku State University, General and Inorganic Chemistry Department, AZ1148 Baku, Azerbaijan*
[6]*Institute of Geology and Mineralogy SB RAS, 630090 Novosibirsk, Russia*
[7]*Institute of Semiconductor Physics SB RAS, and Novosibirsk State University, 630090 Novosibirsk, Russia*
[8]*Departamento de Física de Materiales UPV/EHU, Centro de Física de Materiales CFM—MPC and Centro Mixto CSIC-UPV/EHU, 20080 San Sebastián/Donostia, Spain*
[9]*Department für Geowissenschaften Ludwig-Maximilians Universität München, D-80333 München, Germany*
[10]*Institut für Physik, Martin-Luther-Universität Halle-Wittenberg, D-06099 Halle, Germany*

(Received 12 May 2014; published 9 September 2014)

Angular resolved photoemission spectroscopy in combination with *ab initio* calculations show that trace amounts of carbon doping of the Bi_2Se_3 surface allows the controlled shift of the Dirac point within the bulk band gap. In contrast to expectation, no Rashba-split two-dimensional electron gas states appear. This unique electronic modification is related to surface structural modification characterized by an expansion of the top Se-Bi spacing of ≈11% as evidenced by surface x-ray diffraction. Our results provide new ways to tune the surface band structure of topological insulators.

DOI: 10.1103/PhysRevLett.113.116802 PACS numbers: 73.20.At, 61.05.cp, 71.15.Mb, 79.60.-i

Three-dimensional topological insulators (TIs) are nonmagnetic semiconductors that host metallic surface states originating from a bulk energy band gap inversion driven by spin-orbit coupling [1–3]. These topological surface states (TSSs) form a Dirac cone in which the spin of an electron is locked perpendicular to its momentum thus being protected from the elastic backscattering, a property provided by time-reversal symmetry. In such a way, TSSs are robust against disorder or perturbation, which respects time-reversal symmetry. This has been confirmed by scanning tunneling microscopy and spectroscopy experiments on the random alloy $Bi_{0.92}Sb_{0.08}$ [4] surface, and defected Bi_2Se_3 and Bi_2Te_3 surfaces [5–7]. This remarkable property of topological protection makes TIs potentially promising materials for realization of dissipationless spin transport [8,9].

Topological protection also manifests itself in the experiments where various adsorbates have been deposited. It has been shown recently [10], that the TSS remains unchanged until the concentration of adatoms reaches the level at which the Fermi surface contours acquire strong hexagonal warping, regardless of whether the adsorbates are magnetic or nonmagnetic. Several photoemission studies have shown the appearance of the two-dimensional electron gas (2DEG) states at the Bi_2Se_3 surface exposed to molecules [11–13] or various adatoms [13–17]. In particular, the parabolic bands with a Rashba splitting are formed in the energy gap just below the bulk conduction band. Overlapping with TSS in a certain energy range, these spin-polarized states represent a natural scattering channel for the TSS carriers. This can degrade transport characteristics of the adsorbate-covered TI surfaces as compared to the clean ones, hampering their possible application in devices based on the topological spin currents.

In this Letter, we show for the first time that dosing of the TI surfaces with a certain kind of adsorbate not only avoids the appearance of undesirable states in the band gap, but even can be used for tuning the TSSs. The latter is feasible via the controllable expansion of the first interlayer spacing (d_{12}) which can be achieved, e.g., by doping the Bi_2Se_3 surface with carbon. Indeed, the surface x-ray diffraction (SXRD) experiments and *ab initio* calculations revealed that carbon atoms penetrate inside the topmost quintuple layer (QL) of Bi_2Se_3 and induce an expansion of $\Delta d_{12}/d_{12} \approx 11\%$. Further angle-resolved photoemission spectroscopy (ARPES) measurements found no evidence of the Rashba-split 2DEG states, but instead featured an upward energy shift of the Dirac point (DP) inside the bulk band gap, in agreement with *ab initio* electronic structure calculations. These results show that the DP position inside the TI band gap can be controlled by virtue of specific surface doping. Since the latter does not involve the formation of undesirable trivial states in the TI band gap, such an approach makes the adsorbate-covered TIs attractive for possible applications.

The Bi_2Se_3 samples were grown by the Bridgman method. After transfer into the ultrahigh vacuum (UHV),

the surface was cleaned by mild Ar^+ ion sputtering ($E = 0.5 - 1$ keV) followed by annealing up to 470 °C. The surface is clean on the basis of Auger electron spectroscopy (AES) and exhibits a high contrast low-energy electron diffraction pattern with sharp spots reflecting the $p3m1$ plane group symmetry. Doping of the as-prepared surface by carbon was carried out by dosing 8.4×10^4 L (1 L = 10^{-6} Torr s) of C_4H_6 under simultaneous irradiation with electrons ($E_{kin} = 500$ eV) emitted from a flood gun (sample current ≈600 μA). We emphasize that the latter induces the cracking of the C_4H_6 molecules leaving carbon atoms in the near-surface region. Dosing of C_4H_6 alone is not sufficient to deposit carbon in detectable amounts. The SXRD experiments were carried out *in situ* in an UHV surface x-ray diffractometer equipped with a microfocus x-ray source (Cu-$K\alpha$) and a two-dimensional (2D) pixel detector [18]. Laboratory (LAB) experiments were complemented by experiments at the beam line 25B of the European Synchrotron Radiation Facility (ESRF) in Grenoble (France) also using 2D detector and 14 keV x rays.

In Figs. 1(a) and 1(b) symbols and lines correspond to the experimental ($|F_{obs}(hk\ell)|$) and calculated ($|F_{calc}(hk\ell)|$) structure factor amplitudes along four crystal truncation rods (CTRs) of the clean $Bi_2Se_3(0001)$ surface. Data taken at the ESRF (a) and in the LAB (b) were derived from the integrated intensities $[I(hk\ell)]$ with $\sqrt{I(hk\ell)} \propto |F_{obs}(hk\ell)|$ collected under grazing incidence [$\alpha_i = 0.3°$ (LAB) and $\alpha_i = 1.0°$ (ESRF)] of the incoming beam. According to the hexagonal setting of the rhombohedral crystal structure bulk Bragg reflections appear at the condition $-h + k + \ell = 3n$ ($n \in \mathbb{Z}$). Several LAB data sets were collected, in general each consisting of about 160 symmetry independent reflections. The ESRF data set consists of 1079 reflections along five CTRs. The ESRF and LAB data are remarkably reproducible.

Uncertainties (1σ) of the $|F_{obs}(hk\ell)|$ represented by the error bars were derived from the counting statistics. Fits were carried out by minimizing the unweighted R value (R_u) [19]. Since selenium and bismuth occupy high site symmetry positions in the $p3m1$ plane group [20], only the z parameters of the atoms (one independent atom per layer) are free structural parameters. In addition, one overall isotropic Debye parameter $B = 8\pi\langle u^2\rangle$ was allowed to vary, where $\langle u^2\rangle$ represent the mean squared displacement amplitude. Good fits could be achieved. We obtain R_u in the range between ≈12% and 14%.

Figure 2 shows a schematic structure model in side view. On the right the relaxations of the interlayer spacings relative to the bulk [20] are indicated. Relaxations are found to be significant within the uppermost QL layer only. The structure parameters derived from the ESRF and LAB data for the un-doped sample are in good agreement, especially with regard to the top interlayer expansion $\Delta d_{12}/d_{12}$. It is +1.8% for ESRF and +2.7% for the LAB data ($d_{12} = 1.578$ Å). There is also some evidence for a slight contraction of the second spacing ($\Delta d_{23}/d_{23} = -1.7\%$, LAB: −2.4%), while the deeper ones are almost unrelaxed. The only larger disagreement ≈3%, corresponding to 0.07 Å between the ESRF and the

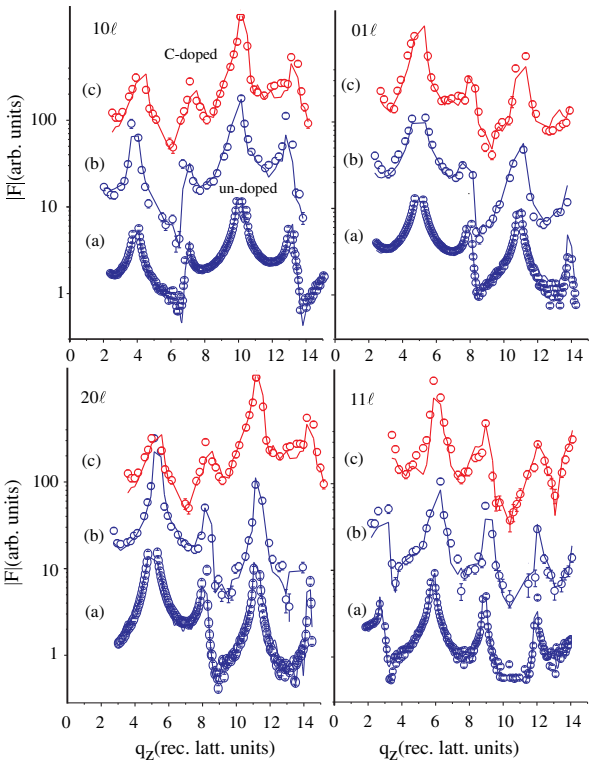

FIG. 1 (color online). Experimental (symbols) and calculated (lines) structure factor amplitudes $|F(hk\ell)|$ along four CTRs, 10ℓ, 01ℓ, 20ℓ, and 11ℓ, for the clean $Bi_2Se_3(0001)$, as measured at the ESRF (a) and in the LAB (b), as well as those for carbon doped $Bi_2Se_3(0001)$ as acquired in the LAB (c). Curves are shifted for clarity.

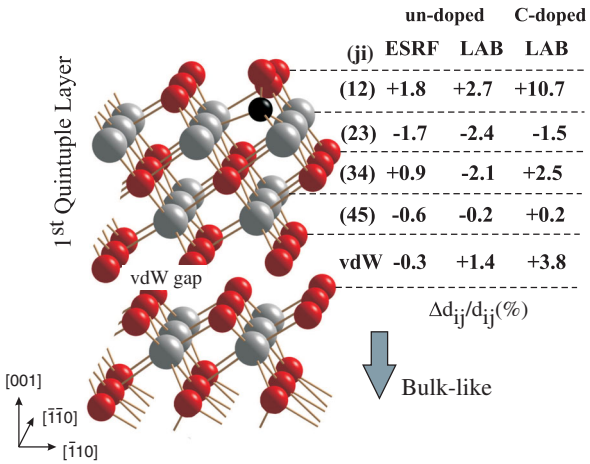

FIG. 2 (color online). Model of the Bi_2Se_3 near-surface structure. Red (small) and gray (large) spheres represent Se and Bi atoms, respectively. Interlayer spacings relative to the bulk are labeled on the right for the different data sets. Carbon (small black sphere) is placed in the most favorable position according to the *ab initio* calculations.

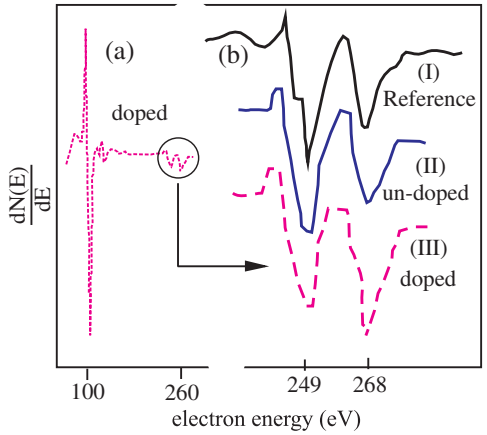

FIG. 3 (color online). (a) Differential AES spectrum showing the Bi-NOO (96 and 101 eV) and the Bi-NNO transitions (249 and 268 eV) of the doped Bi_2Se_3 sample. (b) Zoom into the 250 to 270 eV regime: (I) reference reproduced from Ref. [22], (II) undoped sample, and (III) carbon-doped sample.

LAB data is observed for $\Delta d_{34}/d_{34}$. This worst case is used as an estimate for the uncertainty for the determination of Δd_{ij} in general. An analysis of the variance of R_u upon variation of the structure parameters leads to about the same value [21]. The magnitude of the Debye parameter lies in the normal range for surfaces ($B \approx 2$–5 Å^2).

AES spectra (electron energy $E_p = 3$ keV) taken for the doped Bi_2Se_3 surface clearly indicate the presence of carbon, albeit at very small amounts as estimated by comparison of the AES spectra shown in Fig. 3. Figure 3(a) shows a differential AES spectrum of doped Bi_2Se_3 including the Bi peaks between 96 and 268 eV. Note that the sensitivity of the (unresolved) NOO lines at 96 and 101 eV is roughly a factor of 8 larger than that of the NNO lines in the 249 to 268 eV range [22]. We note that the 96/101 eV lines are correctly labeled as $N_{6,7}O_{4,5}O_{4,5}$, but for short we use the term NOO for these. Figure 3(b) shows a zoom into the 250–270 eV regime. The solid upper curve (I) represents the differential AES spectrum in the vicinity of the Bi-NNO lines at 249 and 268 eV taken from Ref. [22]. Spectrum (II) corresponds to the AES peaks obtained from the un-doped sample, while spectrum (III) was obtained after doping with carbon. The carbon KLL peak is located at $E_{\mathrm{kin}} \approx 272$ eV; therefore, it cannot be separated from the Bi-NNO line at $E_{\mathrm{kin}} = 268$ eV. However, after carbon doping there is a small increase of the peak at $E_{\mathrm{kin}} = 268$ eV relative to that at $E_{\mathrm{kin}} = 248$ eV which is attributed to the presence of carbon. The sensitivity of the carbon KLL peak for $E_p = 3$ keV is approximately a factor of 3 larger than that of the Bi-NNO peaks [22]. We estimate the amount of carbon to be well below half a monolayer.

The upper curves (red) labeled by (c) in Fig. 1 represent the $|F(hk\ell)|$ of the carbon-doped sample collected in the LAB experiment. The corresponding structure parameters are listed on the right of Fig. 2. There is a pronounced expansion of $\Delta d_{12} = 11\%$, while the other interlayer spacings remain unrelaxed within the experimental uncertainty of $\pm 3\%$. Direct inspection of the CTRs in Fig. 1 shows significant differences especially near the antiphase position in between the bulk Bragg reflections. The expansion of d_{12} in the 10% range is reproduced for a number of samples [23] and depends sensitively on the degree of carbon doping. For more details we refer to the Supplemental Material [24].

Since SXRD is not sensitive to low-Z elements like carbon, *ab initio* calculations were carried out to determine a possible location of carbon atoms. We employed the projector augmented-wave method [25] in VASP implementation [26,27] and the generalized gradient approximation to the exchange-correlation potential [28]. The

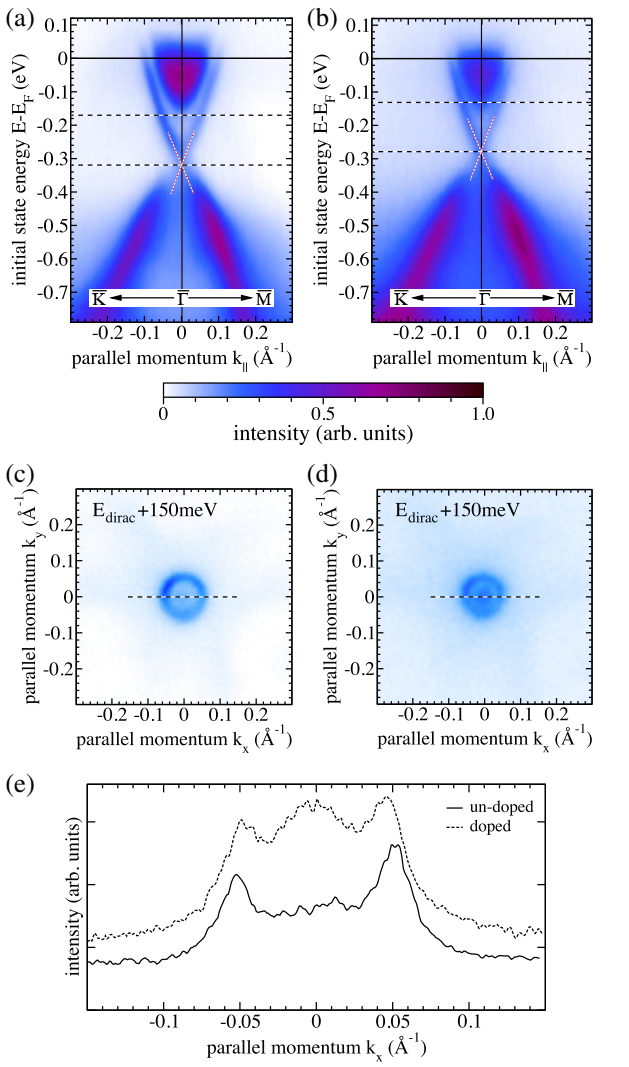

FIG. 4 (color online). Momentum-resolved photoemission measurement: band dispersion of undoped (a) and carbon-doped (b) Bi_2Se_3 along the $\bar{K} - \bar{\Gamma}$ and $\bar{\Gamma} - \bar{M}$ direction. Dotted straight lines serve as a guide to the eye to the band dispersion in the vicinity of the DP. Binding energies are given relative to the Fermi level (E_F). Horizontal lines indicate the energy of the DP and the $k_{\|}$ contour for the undoped (c) and doped (d) samples. (e) Intensity profiles along the dashed line in (c) and (d).

calculations were carried out by using 2 QL-thick Bi_2Se_3 films and placing one carbon atom per $(3 \times 2\sqrt{3})$ rectangular supercell with 12 atoms per single substrate layer, which is equivalent to an impurity concentration of ~8.3%. Several high-symmetry surface adsorption sites (top, bridge, fcc-, and hcp-hollow) were considered, as well as interstitials and positions inside the van der Waals (vdW) gap. In all cases, atomic coordinates were relaxed until the forces were less than 5×10^{-2} eV/Å. We found that carbon strongly prefers the interstitial site between the first and second layer (see Fig. 2). This geometry is by at least 0.69 eV more favorable than any other, and leads to a ~6% increase of the *average* d_{12}. This value is less than the experimental one; however, we attribute this to the comparatively lower concentration of carbon (8.3%) assumed in the calculation.

To explore the effect of carbon doping on the Bi_2Se_3 surface electronic structure, ARPES experiments were performed at room temperature. The surface was illuminated along the $\bar{M} - \bar{\Gamma} - \bar{M}$ direction by He-I ($h\nu = 21.23$ eV) radiation emitted from a focused gas discharge lamp, under an angle of incidence of 22° with respect to the sample surface. Photoelectrons emitted into the 2π solid angle above the surface were collected by the objective lens of a photoelectron emission microscope, forming a crystal momentum (k_x, k_y) resolved image of the photoelectron intensity distribution. Series of constant energy vs momentum images (energy resolution ~20 meV) were recorded by a CCD camera from a fluorescent screen image detector.

Figure 4(a) shows the ARPES spectrum of the pristine $Bi_2Se_3(0001)$ surface along the $\bar{K} - \bar{\Gamma}$ and $\bar{\Gamma} - \bar{M}$ direction. As is usually observed for naturally grown Bi_2Se_3, the DP is located 320 meV below E_F, which is fixed due to n doping by selenium vacancies and traverses the conduction band. Note, that E_F can be shifted down into the energy gap by a very slight bulk calcium doping [16].

The spectrum obtained for the carbon-doped surface is shown in Fig. 4(b). First of all, there is some band broadening (see, e.g., the extra wings apparent in the valence band between −0.3 and −0.5 eV), which we relate to the presence of disordered carbon. More importantly and in contrast to expectation, carbon doping does not lead to a formation of Rashba-split 2DEG states in the Bi_2Se_3 band gap. In Ref. [17] it has been argued that such states appear due to the near-surface electrostatic potential variation induced by adsorption of foreign species on the surface. However, it turns out to not be the case for the carbon-doped Bi_2Se_3 surface, whose TSS is thus protected against possible spin-dependent scattering into trivial states. We observe an upward shift of the DP by 40 ± 20 meV. This is best seen in the constant energy contour of the surface state, displayed at an energy of 150 meV above the DP, as shown in Figs. 4(c) and 4(d) for the undoped and doped sample, respectively. While this energy is below the conduction band minimum for the undoped sample, i.e., the circular contour of the surface state is unfilled, significant additional intensity from the conduction band is present for the carbon-doped sample [see also the horizontal intensity profiles along the dashed line in Fig. 4(e)].

To uncover the reason of such a DP shift we performed *ab initio* electronic structure calculations. Since carbon doping does not lead to the appearance of trivial bands inside the Bi_2Se_3 band gap, one can assume that such changes are of pure structural origin. Since the carbon adsorption induced expansion of the top layer spacing is the dominating structural modification, a set of surface electronic structure calculations was carried out for different expansions, while keeping all other structure parameters fixed at experimental values. The band structure of the unperturbed $Bi_2Se_3(0001)$ surface is shown in Fig. 5(a). It is characterized by a spin-polarized TSS with the DP at E_F, which resides near the valence band maximum. In agreement with the ARPES measurements, an upward shift of the DP is observed for $\Delta d_{12}/d_{12} = 10\%$. The only difference with respect to the experiment is the magnitude of the shift (100 meV), moving the DP almost to the center of the bulk band gap [Fig. 5(b)]. Thus, the upward shift of the DP

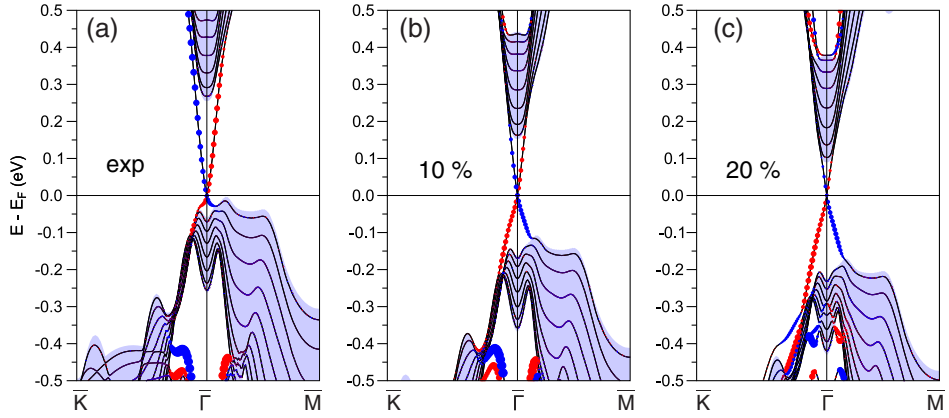

FIG. 5 (color online). Band structure of $Bi_2Se_3(0001)$ calculated for several expansions, $\Delta d_{12}/d_{12}$. (a): Structure from SXRD, $\Delta d_{12}/d_{12} = 3\%$, (b): 10%, (c): 20%. Red and blue lines indicate spin up and spin down states, respectively. The shaded area corresponds to the bulk states.

of the carbon-doped Bi_2Se_3 surface is directly related to the top interlayer expansion. An upper limit of $\Delta d_{12}/d_{12} = 20\%$ is found up to which the DP is still located at E_F and the TSS spin polarization is maintained (see Fig. 5(c) and the Supplemental Material [24]).

In summary, we have shown that the position of the DP within the TI band gap can be controlled by surface doping. By means of suitable adsorbate choice (in the present work—carbon) and under specific doping conditions it is possible to expand the first interlayer spacing of the TI substrate in controllable fashion, thus positioning the DP in the band gap. Other ways to control the position of the DP have been previously proposed. The effect of *local strains* at grain boundaries in Bi_2Se_3 has been shown to influence the position of the DP in a very recent study [29]. In contrast, DP tuning by carbon doping is achieved homogeneously across the macroscopic surface, which is important for possible applications. The variation of *bulk* atomic composition [30,31], or preparing heterostructures, consisting of a thin semiconducting overlayer on top of the TI substrates [32], were also proposed to tune a DP. The former approach requires preparation of complex ternary [30] or quaternary [31] TI compounds, while the latter requires highly controllable epitaxial growth. By contrast, the method of the DP position control proposed in the present work does not require any intricate growth procedure and can be applied to the tetradymite-like TI compounds which are relatively simple to grow. Our study suggests a new path to actively modify the TSS by virtue of the specific surface doping which does not degrade the TI electronic spectrum.

This work is supported by the DFG through Priority Program "Topological Insulators (SPP 1666)" and by Science Development Foundation under the President of the Republic of Azerbaijan [Grant No. EIF-2011-1(3)-82/69/4-M-50]. We acknowledge the help of G. Castro, J. Rubio-Zuazo, and J. Drnec during the experiments at the ESRF. We thank F. Weiss for technical support. Calculations were performed at the SKIF-Cyberia supercomputer of Tomsk State University.

*hmeyerhm@mpi-halle.de

[1] L. Fu, C. L. Kane, and E. J. Mele, Phys. Rev. Lett. **98**, 106803 (2007).
[2] Y. Xia, D. Qian, D. Hsieh, L. Wray, A. Pal, H. Lin, A. Bansil, D. Grauer, Y. S. Hor, R. J. Cava *et al.*, Nat. Phys. **5**, 398 (2009).
[3] H. Zhang, C.-X. Liu, X.-L. Qi, X. Dai, Z. Fang, and S.-C. Zhang, Nat. Phys. **5**, 438 (2009).
[4] P. Roushan, J. Seo, C. V. Parker, Y. S. Hor, D. Hsieh, D. Qian, A. Richardella, M. Z. Hasan, R. J. Cava, and A. Yazdani, Nature (London) **460**, 1106 (2009).
[5] T. Hanaguri, K. Igarashi, M. Kawamura, H. Takagi, and T. Sasagawa, Phys. Rev. B **82**, 081305 (2010).
[6] Z. Alpichshev, J. G. Analytis, J.-H. Chu, I. R. Fisher, Y. L. Chen, Z. X. Shen, A. Fang, and A. Kapitulnik, Phys. Rev. Lett. **104**, 016401 (2010).
[7] P. Sessi, M. M. Otrokov, T. Bathon, M. G. Vergniory, S. S. Tsirkin, K. A. Kokh, O. E. Tereshchenko, E. V. Chulkov, and M. Bode, Phys. Rev. B **88**, 161407(R) (2013).
[8] M. Z. Hasan and C. L. Kane, Rev. Mod. Phys. **82**, 3045 (2010).
[9] X.-L. Qi and S.-C. Zhang, Rev. Mod. Phys. **83**, 1057 (2011).
[10] T. Valla, Z.-H. Pan, D. Gardner, Y. S. Lee, and S. Chu, Phys. Rev. Lett. **108**, 117601 (2012).
[11] H. M. Benia, C. Lin, K. Kern, and C. R. Ast, Phys. Rev. Lett. **107**, 177602 (2011).
[12] C. Chen, S. He, H. Weng, W. Zhang, L. Zhao, H. Liu, X. Jia, D. Mou, S. Liu, J. He *et al.*, Proc. Natl. Acad. Sci. U.S.A. **109**, 3694 (2012).
[13] P. D. C. King, R. C. Hatch, M. Bianchi, R. Ovsyannikov, C. Lupulescu, G. Landolt, B. Slomski, J. H. Dil, D. Guan, J. L. Mi *et al.*, Phys. Rev. Lett. **107**, 096802 (2011).
[14] Z.-H. Zhu, G. Levy, B. Ludbrook, C. N. Veenstra, J. A. Rosen, R. Comin, D. Wong, P. Dosanjh, A. Ubaldini, P. Syers *et al.*, Phys. Rev. Lett. **107**, 186405 (2011).
[15] M. Ye, S. V. Eremeev, K. Kuroda, M. Nakatake, S. Kim, Y. Yamada, E. E. Krasovskii, E. V. Chulkov, M. Arita, H. Miyahara *et al.*, arXiv:1112.5869.
[16] M. Bianchi, R. C. Hatch, Z. Li, P. Hofmann, F. Song, J. Mi, B. B. Iversen, Z. M. Abd El-Fattah, P. Löptien, L. Zhou *et al.*, ACS Nano **6**, 7009 (2012).
[17] M. Bahramy, P. King, A. De La Torre, J. Chang, M. Shi, L. Patthey, G. Balakrishnan, P. Hoffmann, R. Arita, N. Nagaosa *et al.*, Nat. Commun. **3**, 1159 (2012).
[18] C. M. Schlepütz, R. Herger, P. R. Willmott, B. D. Patterson, O. Bunk, C. Brönnimann, B. Henrich, G. Hülsen, and E. F. Eikenberry, Acta Crystallogr. Sect. A **61**, 418 (2005).
[19] $R_u = \sum ||F_{obs}| - |F_{calc}|| / \sum |F_{obs}|$. Here, F_{obs}, F_{calc} are the experimental and calculated structure factors, respectively. The summation runs over all data points.
[20] C. Vicente, P. J. L. Tirado, K. Adouby, J. C. Jumas, A. A. Touré, and G. Kra, Inorg. Chem. **38**, 2131 (1999).
[21] W. C. Hamilton, Acta Crystallogr. **18**, 502 (1966).
[22] L. E. Davis, N. C. MacDonald, P. W. Palmberg, G. E. Riach, and R. E. Weber, *Handbook of Auger Electron Spectroscopy* (Physical Electronics Industries, Eden Prairie, MN, 1976).
[23] S. Roy, H. L. Meyerheim, K. Mohseni, A. Ernst, G. Mussler, J. Kampmeier, D. Grützmacher, J. Schneider, E. Chulkov, and J. Kirschner (to be published).
[24] See Supplemental Material at http://link.aps.org/supplemental/10.1103/PhysRevLett.113.116802 for top layer expansion versus carbon doping and for ARPES spectra versus carbon doping.
[25] P. E. Blöchl, Phys. Rev. B **50**, 17 953 (1994).
[26] G. Kresse and J. Furthmüller, Comput. Mater. Sci. **6**, 15 (1996).
[27] J. Hafner, J. Comput. Chem. **29**, 2044 (2008).
[28] J. P. Perdew, K. Burke, and M. Ernzerhof, Phys. Rev. Lett. **77**, 3865 (1996).
[29] Y. Liu, Y. Y. Li, S. Rajput, D. Gilks, L. Lari, P. L. Galindo, M. Weinert, V. K. Lazarov, and L. Li, Nat. Phys. **10**, 294 (2014).
[30] J. Zhang *et al.*, Nat. Commun. **2**, 574 (2011).
[31] T. Arakane, T. Sato, S. Souma, K. Kosaka, K. Nakayama, M. Komatsu, T. Takahashi, Z. Ren, K. Segawa, and Y. Ando, Nat. Commun. **3**, 636 (2012).
[32] T. V. Menshchikova, M. M. Otrokov, S. S. Tsirkin, D. A. Samorokov, V. V. Bebneva, A. Ernst, V. M. Kuznetsov, and E. V. Chulkov, Nano Lett. **13**, 6064 (2013).